VŠB — Technická univerzita Ostrava
Univerzitní studijní programy
Institut fyziky

Struktura a vlastnosti CoSiB/FeSiB slitin perspektivních pro dvouvrstvé senzory

Structure and properties of CoSiB/FeSiB alloys perspective for bilayered sensors

Student: Andrii Titov
Vedoucí bakalářské práce: Ing. Ondřej Životský, Ph.D.
Konzultant: Ing. Yvonna Jirásková, Ph.D.

VŠB - Technical University of Ostrava
University Study Programmes
Institute of Physics

Bachelor Thesis Assignment

Student:	**Andrii Titov**
Study Programme:	B3942 Nanotechnology
Study Branch:	3942R001 Nanotechnology
Title:	Struktura a vlastnosti CoSiB/FeSiB slitin perspektivních pro dvouvrstvé senzory Structure and properties of CoSiB/FeSiB alloys perspective for bilayer sensors

Description:

Předmětem bakalářské práce je analýza strukturních a magnetických vlastností dvouvrstvých pásků připravených metodou rovinného lití na měděný válec (planar flow casting - PFC). Jedná se o zcela nové materiály tvořené vrstvami CoSiB z jedné strany a FeSiB ze strany opačné s rozdílnými koeficienty magnetostrikce. Uplatnění těchto materiálů se předpokládá v oblasti detekce a monitorování teplotních změn, případně v medicínských aplikacích např. při měření tlaku krve.
Výsledky dosažené na dvouvrstvých páscích budou konfrontovány se strukturními a fyzikálními vlastnostmi pásků CoSiB a FeSiB připravených stejnou technologií. Kombinace experimentálních metod na Institutu fyziky (VŠB-TUO) a Ústavu fyziky materiálů (AVČR v. v. i., Brno, konzultant Dr. Y. Jirásková) dává předpoklad k dosažení komplexních informací o těchto nových materiálech, které by, mimo jiné, mohly přispět výrobci k případné změně technologických parametrů a vylepšení technologie přípravy dvouvrstvých pásků požadovaných vlastností.

Řešení práce je možné rozdělit do následujících bodů:

1. Detailní seznámení se s technologií přípravy rychle chlazených materiálů (PFC) ve formě pásků, a to jak CoSiB a FeSiB, tak dvouvrstvých slitin CoSiB/FeSiB. Studiem literatury získat přehled o strukturních a fyzikálních vlastnostech těchto materiálů.

2. Strukturní a fázová analýza jejich objemu a povrchu pomocí metod rentgenové difrakce (XRD), vysokorozlišovací skenovací elektronové mikroskopie (HRSEM), transmisní elektronové mikroskopie (TEM) a Mössbauerovy spektroskopie (MS).

3. Studium objemových magnetických vlastností (např. kritických fázových přeměn a Curieovy teploty) pomocí magnetometru s vibrujícím vzorkem (VSM) a povrchových magnetických vlastností (hysterézních smyček a doménové struktury) s využitím magnetooptického Kerrova jevu (MOKE).

4. Charakterizace rozhraní dvouvrstvých slitin CoSiB/FeSiB.

The aim of bachelor thesis is the analysis of structural and magnetic properties of bilayer ribbons prepared by planar flow casting (PFC) method. They are new materials consisting of CoSiB layer from one side and FeSiB layer from the opposite side with different magnetostriction coefficients. Their practical usage is anticipated in the field of detection and monitoring of temperature changes, eventually in medical applications e.g. at blood pressure measurements.
Obtained results of bilayer ribbons will be compared with structural and physical properties of original CoSiB and FeSiB alloys prepared by the same technology. Combination of experimental methods at Institute of Physics (VŠB-TUO) and Institute of Physics of Materials (AVČR v. v. i., Brno, consultant Dr. Y. Jirásková) will give us complex information about these materials that should, among other things, contribute the producer to the prospective changes of technological parameters and preparation of bilayer ribbons with desired properties.

Solution of the thesis can be distinguished into the following points:

1. Detail acquainting with preparation technology (PFC) of CoSiB, FeSiB, and bilayer CoSiB/FeSiB ribbons. Make a recherché of literature focused on the structural and physical properties of these materials.

2. Structural and phase analysis of their volume and surface using the methods of X-ray diffraction (XRD), high resolution scanning electron microscopy (HRSEM), transmission electron microscopy (TEM) a Mössbauer spectroscopy (MS).

3. Study of volume magnetic properties (e.g. critical phase transformations and Curie temperature) by the vibrating sample magnetometer (VSM) and surface magnetic properties (hysteresis loops and domain structure) using the magneto-optical Kerr effect (MOKE).

4. Characterization of interface in bilayer CoSiB/FeSiB alloys.

References:

Glassy Metals I, eds. H.-J. Güntherodt, H. Beck, Topics in Applied Physic, Vol. 46, Springer-Verlag, Berlin Heidelberg New York, 1981.

Glassy Metals II, eds. H. Beck, H.-J. Güntherodt, Topics in Applied Physic, Vol. 53, Springer-Verlag, Berlin Heidelberg New York Tokio, 1983.

A. Hubert, R. Schäfer, Magnetic domains – The analysis of magnetic microstructures, Springer-Verlag, Berlin Heidelberg New York, 1998.

A. Mitra, R. K. Roy, B. Mahato, A. K. Panda, G. Vlasák, D. Janičkovič, P. Švec Sr., Development of FeSiB/CoSiB Bilayered Melt-spun Ribbon by Melt-spinning Technique, J. Supercond. Nov. Magn. 24, 611-615, 2011.

Extent and terms of a thesis are specified in directions for its elaboration that are opened to the public on the web sites of the faculty.

Supervisor: **Ing. Ondřej Životský, Ph.D.**

Consultant: Dr. Yvonna Jirásková

Date of issue: 16. 11. 2012

Date of submission: 15. 05. 2013

prof. Dr. RNDr. Jiří Luňáček
Head of Department

VYSOKÁ ŠKOLA BÁŇSKÁ - TECHNICKÁ UNIVERZITA OSTRAVA UNIVERZITNÍ STUDIJNÍ PROGRAMY

prof. Ing. Petr Noskievič, CSc.
Vice-rector for Study Affairs

Prohlášení

- *Byl jsem seznámen s tím, že na moji bakalářskou práci se plně vztahuje zákon č. 121/2000 Sb. — autorský zákon, zejména §35 - využití díla v rámci občanských a náboženských obřadů, v rámci školních představení a využití díla školního a §60 — školní dílo.*
- *Beru na vědomí, že Vysoká škola báňská – Technická univerzita Ostrava (dále jen VŠB–TUO) má právo nevýdělečně, ke své vnitřní potřebě, bakalářskou práci užít (§35 odst. 3).*
- *Souhlasím s tím, že jeden výtisk bakalářské práce bude uložen v Ústřední knihovně VŠB–TUO k prezenčnímu nahlédnutí a jeden výtisk bude uložen u vedoucího bakalářské práce. Souhlasím s tím, že údaje o bakalářské práci, obsažené v Záznamu o závěrené práci, umístěném v příloze mé bakalářské práce, budou zveřejněny v informačním systému VŠB–TUO.*
- *Bylo sjednáno, že s VŠB–TUO, v případě zájmu z její strany, uzavřu licenční smlouvu s oprávněním užít dílo v rozsahu §12 odst. 4 autorského zákona.*
- *Bylo sjednáno, že užít své dílo — bakalářskou práci nebo poskytnout licenci k jejímu využití mohu jen se souhlasem VŠB–TUO, která je oprávněna v takovém případě ode mne požadovat přiměřený příspěvek na úhradu nákladů, které byly VŠB–TUO na vytvoření díla vynaloženy (až do jejich skutečné výše).*
- *Místopřísežně prohlašuji, že celou bakalářskou práci včetně příloh, jsem vypracoval samostatně a uvedl jsem všechny použité podklady a literaturu.*

V Ostravě dne 15.5.2013

Andrii Titov

Gratitude

This work has been elaborated in the framework of the Nanotechnology, the basis for international cooperation project, reg. no. CZ.1.07/2.3.00/20.0074 supported by Operational Programme Education for competitiveness supported by Structural Funds of the European Union and state budget of the Czech Republic.

I would like to express my thanks to Ing. Ondřej Životský, Ph.D., an adviser of my bachelor's work. Only under his professional and tactful leadership this work could appear.

I would like to express also my thanks to Dr. Yvonna Jirásková and her colleagues at the Institute of Physics of Materials, AS CR Brno, for possibility to become acquainted with Mössbauer spectroscopy, scanning electron microscopy, and magnetic measurements using VSM and for fruitful discussions.

Abstrakt

Hlavním cílem práce je detailní analýza dvouvrstvého CoSiB/FeSiB pásku a porovnání jeho strukturních a fyzikálních vlastností s vlastnostmi jednovrstvých pásků CoSiB a FeSiB. Pásky byly připraveny rychlým tuhnutím taveniny metodou rovinného lití. Mikrostrukturní a magnetické vlastnosti, studované z hlediska povrchu pásku, objemu a rozhraní mezi vrstvami, byly zkoumány kombinací v současnosti široce používaných experimentálních metod. V práci je ukázáno, že magnetické vlastnosti dvouvrstvého pásku jsou určeny především FeSiB vrstvou. Spojení dvou materiálů s odlišnými magnetostrikcemi a vytvoření difuzní mezivrstvy se jeví jako slibné v senzorových aplikacích.

Klíčová slova: Dvouvrstvé pásky, mikrostruktura, magnetismus, povrchové a objemové vlastnosti

Abstract

The aim of this work is a detailed analysis of bilayered CoSiB/FeSiB ribbons and a comparison of its properties with structural and physical properties of the single-layered FeSiB and CoSiB ribbons. All ribbons were prepared by rapid solidification of a melt using planar flow casting method. Microstructural and magnetic properties, from the viewpoint of ribbon surface, bulk and interface, were investigated by combination of various experimental methods. In the work it is shown that magnetic properties are determined predominantly by FeSiB layer. Moreover, the interconnection of two materials of different magnetostriction behavior and a formation of diffuse interlayer bring new features potentially available for sensing elements.

Keywords: Bilayered ribbons, microstructure, magnetism, surface and bulk properties

Contents

List of signs and symbols

Symbol	Means
B	hyperfine magnetic induction
ΔB	width of distribution of hyperfine induction
D_{21}	ratio of the second and first lines of sextuplet
E	Young's modulus
H_a	anisotropy field
H_c	coercitive field
I	intensity of γ–ray
M_L	longitudinal magnetization component
M_P	polar magnetization component
M_r	remanent magnetization
M_s	saturation magnetization
M_T	transversal magnetization component
α	angle between the ribbon axis and easy magnetization axis
Γ	energy of Mössbauer transition
Δ	quadrupole splitting
δ	isomer shift
θ	angle between the incident γ–ray beam and magnetic moment
2θ	angle of X–ray's incident
λ	wavelength of light
λ_s	magnetostriction coefficient
σ	stress tensor

List of abbreviations

Abbreviation	Means
AQ	As-Quenched
bcc	body-centered cubic
BL	BiLayered
BLC	BiLayered Co-rich side
BLF	BiLayered Fe-rich side
BSE	Back Scattering Electron
CCD	Charged-Coupled Device
CEMS	Conversion Electron Mössbauer Spectroscopy
EDX	Energy Dispersive X-ray spectroscopy
HRSEM	High Resolution Scanning Electron Microscopy
MOKE	Magneto-Optical Kerr Effect
MS	Mössbauer spectroscopy
PC	Personal Computer
PEM	Photo Elastic Modulator
PFC	Planar Flow Casting
RT	Room Temperature
SE	Secondary Electron
SEM	Scanning Electron Microscopy
SL	Single-Layered
SLC	Single-Layered Co-rich side
SLF	Single-Layered Fe-rich side
TMS	Transmission Mössbauer Spectroscopy
VSM	Vibration Sample Magnetometer
WP	Wollaston Prism
XRD	X-Ray Diffraction
γ-BMS	γ-ray Backscattering Mössbauer Spectroscopy
$\frac{\lambda}{4}$D	quarter-wave plate

1 Introduction

CoSiB and FeSiB alloys belong to a group of materials well-know as metallic glasses. A term metallic glasses means that the structure does not embody any regular atoms ordering and translational symmetry. It is similar to a structure of organic glass which means it is amorphous. The non-crystalline structure of metallic material in a form of thin film was observed already at 1940s, but detailed studies began only in the year 1960 [1, 2]. An interest in metallic glasses consists in their exceptional mechanical and magnetic properties, such as high strength, toughness, corrosion and oxidation resistance, high permeability, good saturation magnetization, and low coercivity. Most of these properties are determined by the amorphous structure. To achieve an amorphous structure is not easy. One of the technologies is rapid cooling of a melted material. A cooling rate has to be so fast that the atoms have no time to order and form crystals, usually 10^6 K/s. Methods how to produce the amorphous structure can be divided into the following groups:

- metal deposition from the gas phase (e.g. vacuum deposition, sputtering, chemical reaction in the gas phase);
- fast solidification of the liquid metals or alloys;
- atom disorder due to formation of high defects (e.g. irradiation, by shock waves);
- metallization (chemical and electrolyte methods).

The most extend technology is the solidification of the melted material by rapid cooling used also for preparation of the first amorphous materials many years ago. Methods of quenching of a liquid precursor exist in several variants allowing preparation of solidified alloy in different form, e.g. drop, wire, thin sheet, or ribbon. The method used for production of materials studied in this work was planar flow casting (PFC). It is a continuous casting method for production of amorphous

alloys in a form of the (20 – 30) μm thick and approximately (1 – 10) mm wide ribbons. Its principle is very simple and it is shown schematically in Fig. 1 a, b.

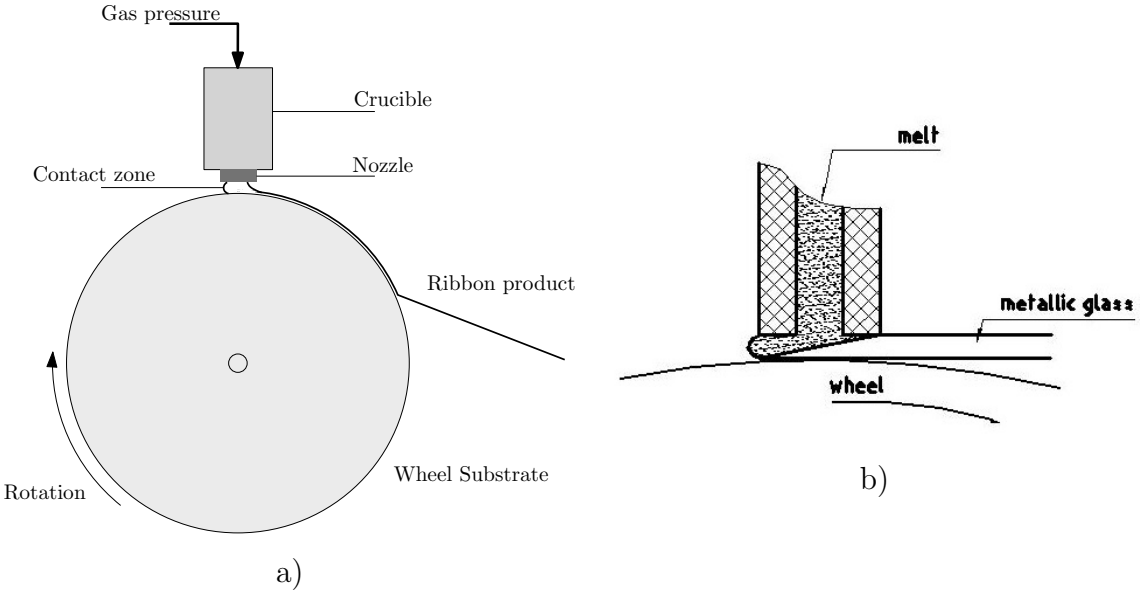

Figure 1: Schematic description of the PFC apparatus

The prepared ingot of desired composition is placed into a crucible made of quartz glass ended by a nozzle of special geometry. The ingot is inductive melted using a high-frequency heating. The crucible is positioned in a certain small distance above a rotating wheel made of copper well dissipating heat. The process shown in Fig. 1 runs in such a way that the melt in the crucible is ejaculated by an inert gas under a certain pressure through the nozzle on the wheel. The nozzle geometry determines a dimension of a ribbon. Because of the small distance between the crucible and the wheel surface a small liquid drop is formed at the nozzle which stabilizes, together with contact pressure, the conditions during casting. The contact between the wheel and a drop is very small nevertheless sufficient to dissipate heat and to allow solidification of the melt. In a laboratory conditions an amount of material is not large (usually 0.5 – 1 kg) and therefore the cooling wheel has not to be additionally cooled, e.g. by water. The wheel rotates with linear velocity and final product is continually removed from the casting zone. The final product is a thin amorphous and/or nanocrystalline ribbon with dimensions mentioned above. The Fig. 2 shows also the other possibilities

of experiment ordering.

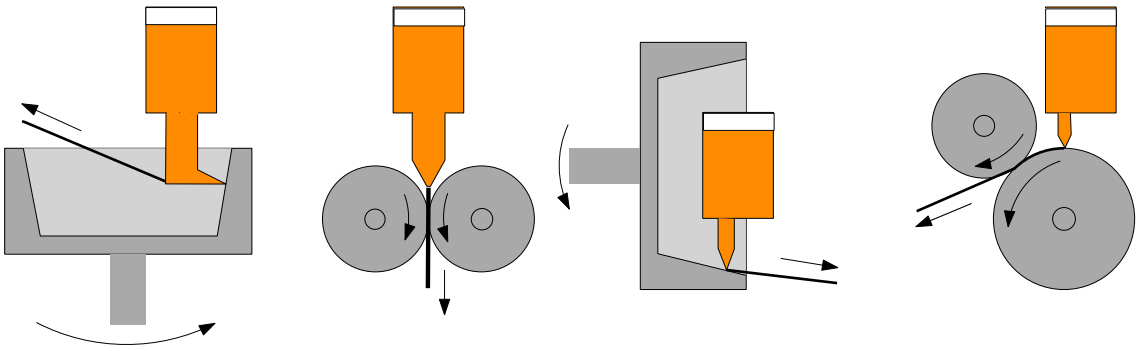

Figure 2: Methods for the preparation a thin ribbons by quenching from the melt

An amorphous structure of alloys prepared by PFC offers very interesting physical properties. For example, most of metallic glasses are characterized by a very high strength and hardness. In amorphous alloys based on iron sub-group (Fe, Co, Ni) HV hardness can reach values higher than 1000, and strength more than 4.0 GNm^{-2} [3]. The value of σ/E reaches for amorphous alloys up to 0.02 – 0.03 while at piano string, as one of the most durable steel product, is this ratio approximately 0.015 [3]. Simultaneously, the metallic glasses yield also high strength and high fracture toughness. Crystalline metals are usually easily destroyed due to cracks along the crystallographic planes and/or crystal boundaries. In amorphous metals, where no crystal structure exists, a fracture owing to cracks was not observed. Nevertheless the fast cooling of the melted material contributes to an origin of stresses in the ribbons having often unfavorable effects on physical properties. They can be removed by so called relaxation heat treatment at ambient temperatures.

From a chemical point of view, the amorphous materials are characterized by various compositions; from the pure metal elements, e.g. Fe, up to materials the composition of which includes more different elements, eg. Co, Fe, Nb, Si. Generally, the amorphous materials consist of metal (Fe, Co) and metalloid (Si, P, B..). A presence of metalloid facilitates an easier formation of amorphous structure. The amorphous

structure is not fully homogenous. It exists a certain short range ordering of atoms into so called clusters which can be different from side to side and therefore we speak about the chemical and topological disorder and/or order of amorphous structure influencing its physical properties. The cluster can be identified with some experimental methods, as e.g. high resolution electron microscopy, Mössbauer spectroscopy, etc. Even if the amorphous structure does not contain defects such as grain boundaries, dislocations, and inclusions known from the crystalline materials, the rapid cooling contributes to formation of free volumes which are comparable with vacancies in crystalline materials. These free volumes can be removed by annealing [3].

The PFC technology conditioned also another feature of the ribbon type materials. During the fast cooling on a rotating wheel, one side of a ribbon is in contact with the wheel surface while the opposite side is in contact with air. This affects the surface microstructure and simultaneously other physical properties, e.g., tendency to surface oxidation or surface crystallization of ribbons influencing very often also the bulk properties of ribbons and consequently determine their possible applications.

The amorphous and/or nanocrystalline materials prepared by PFC method are studied for a long time. Nevertheless the efforts to use this relatively low-costs technology for production of various components are connected with attempts to combine different elements and to prepare amorphous and/or nanocrystalline materials with often unexpected physical properties. Moreover it simulates also a search for preparation of ribbons with enhanced thickness intermediary between classical ribbons and bulk metallic glassy sheets. The higher thickness of ribbons can be achieved by production of bilayered or more layered structures with different or same chemical composition of the layers. The formation of bilayered ribbons is now possible due to slightly modernized technology which uses crucible divided into two parts ended by nozzles close to each other [4, 5, 6]. This allows to ejaculate two melts of different

compositions practically simultaneously and to produce bilayered ribbon as seen in Fig 3.

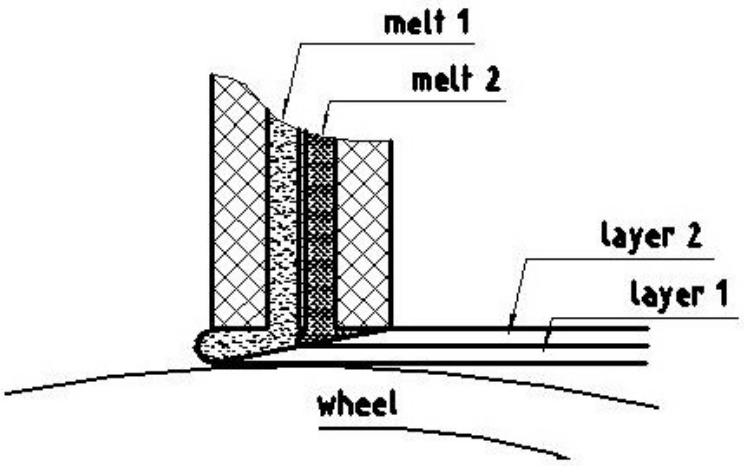

Figure 3: Preparation of bilayered ribbon by the modified PFC method

The aim of the work is to compare the microstructural and magnetic properties of bilayered CoSiB/FeSiB ribbon with the single-layered ones of the same composition. The main reason for this study is the fact that surface, bulk, and interface properties strongly determine possible applications of these alloys.

The absence of crystalline structures enables to use the single-layered amorphous ribbons as small transformers in telecommunication, portable terrestrial field sensors, and secondary current sensors for induction motor control, etc. On the other hand, the stress-impedance properties of bilayered amorphous ribbons can be used in detecting and monitoring bending forces; displacement; temperature changes; in medical applications; in application in the automotive sector [7, 8, 9].

The magnetic properties of as-prepared materials can be further improved by low-temperature treatment and/or by formation of nanocrystallites embedded in amorphous matrix. The nanocrystalline structure of materials can be achieved either by conditions of technology, by composition of material or by additional annealing of as-prepared amorphous ribbon. The temperature treatment can be done also in an external magnetic field influencing alignment of the magnetic moments of annealed

material into one direction which allows further improvement of magnetic properties. In a case of the bilayered ribbon is the situation more complicated. The properties are influenced not only by PFC technology but also mutual combination of materials used.

The first results obtained on bilayered ribbons [7, 10] show their promising use in sensor applications but they have shown also that very intensive basic research, as it concerns materials and their mutual combinations, properties of individual layers and formed interlayer, bulk and surface properties, etc., is highly required. This work should contribute to enlargement of knowledge and bring new information concerning the as-quenched (AQ) bilayered ribbon type materials composed of CoSiB/FeSiB. The whole work consists of four chapters. After the first chapter (Introduction), the chapter 2 is devoted to the material characterization and description of applied experimental techniques. Chapter 3 is focused on the analysis of the ribbon properties from the viewpoint of the surface, bulk, and interface, and finally on the detailed results discussion. The last chapter summarizes obtained results.

2 Experimental

2.1 Material

The investigated bilayered and single-layered ribbons were produced at the Institute of Physics, Slovak Academy of Sciences in Bratislava using the mentioned PFC technique either with the crucible divided into two chambers or with simple crucible. In a case of the bilayered ribbon the experiment was organized in such a way that the CoSiB layer was in a contact with the wheel surface while the FeSiB layer was in contact with air. Therefore the surface from the CoSiB side was matt and the opposite FeSiB surface was shiny. The composition of the layers was $Fe_{77.5}Si_{7.5}B_{15}$ and $Co_{72.5}Si_{12.5}B_{15}$ and with the same composition the single-layered ribbons were prepared. The iron-rich layer has a positive magnetostriction coefficient $\lambda_s \approx 32 \times 10^{-6}$, while the bottom cobalt–rich layer has a negative magnetostrictive coefficient $\lambda_s \approx -2.6 \times 10^{-6}$ [4]. This large difference in magnetostriction coefficients results in a coiling of the bilayered ribbon along the lateral and the transversal directions. The geometrical dimensions of the ribbons were the following: 36 μm thick and 8 mm wide.

In the following text the bilayered (BL) samples will be denoted as BLC for the Co-side and BLF for the Fe-side. The corresponding single-layered samples are denoted SLC and SLF, whereas the measurements are done predominantly from the matt side of the SLC sample and the shiny side of the SLF sample. The geometrical dimensions of SL ribbons were: 20 μm thick and 10 mm wide.

2.2 Electron microscopy

The microstructure and element concentration profiles were obtained using a TESCAN LYRA 3XMU FEG/SEM scanning electron microscope with an Oxford Instruments energy dispersive X-ray analyzer X-Max 80 (EDX). The applied accelerating voltage was 15 kV.

2.3 X-ray diffraction

The microstructure of samples was studied by the X-ray diffraction (XRD) using XPert powder diffractometer. Standard XRD diffractograms were obtained using CoKα ($\lambda = 1.789$ nm) radiation in Bragg-Brentano geometry. γ-rays incident the sample surface at the angles from 24° to 135°. The penetration depth of XRD is approximately 10 μm and the measurements of the BL and SL samples were carried out from both sides: the air and the wheel.

2.4 Raman microspectroscopy

Raman spectroscopy is two-photon inelastic light scattering technique. When the incident photon is of much greater energy than the vibrational quantum energy it loses part of its energy to the molecular vibration with the remaining energy scattered as a photon with reduced frequency [11]. Then the energy shift can provide us the information of the specific chemical bonds in the sample. To determine the surface oxidation in the near-surface area (hundreds of nm) of investigated ribbons the Raman spectra were obtained by confocal Raman microscope XploRA, HORIBA Jobin Yvon with 532 nm excitation laser. Raman spectroscopy was used for determine presence of oxides on the surface of the ribbons.

2.5 Magneto-optical methods

For investigation the surface magnetic properties, square samples were cut out from the ribbons and glued by conducting adhesive on the pin stubs. The studies were carried out on the BLC and BLF sides, and in the case of single-layered samples on the wheel SLC and the air SLF sides. The study of the surface magnetic properties was provided using two magnetic methods, which are based on the magneto-optical Kerr effect (MOKE).

MOKE was discovered and described in 1876 by John Kerr, when he observed the reflection of light from the polished surface of the pole of the magnet. The gist of the MOKE is that the linearly polarized light reflected from a ferromagnetic material becomes elliptically polarized. In this case, the major samiaxis of the ellipse of polarization is rotated by a certain angle relative to the plane of the incident light. The angles of rotation of the reflected elliptically polarized light and the ellipticity describing the ratio of the major and minor semiaxis of the polarization ellipse are proportional to the magnetization of the ferromagnetic material. The incident light beam is usually polarized in the plane of light incidence or parallel to the plane of incidence, because any other polarization complicates appearance of the MOKE [12].

We distinguish three main measurement configurations, which depend on the direction of the vector of the magnetization: polar, longitudinal and transversal, as shown in Figure 4.

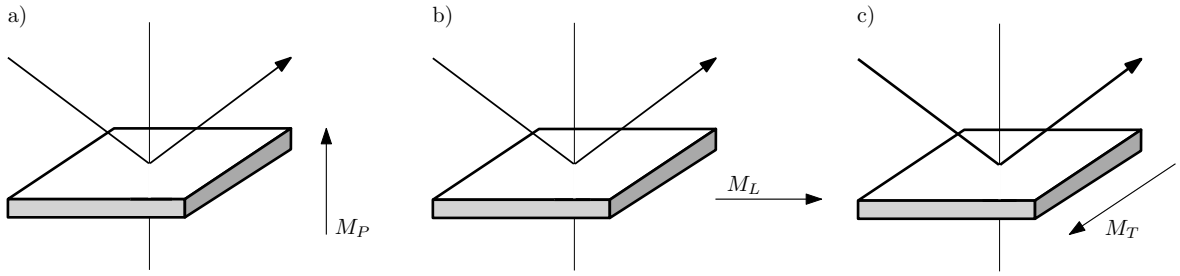

Figure 4: Schematic description of the Kerr effect in reflection: a) polar, b) longitudinal, c) transversal configurations

The first method is arrangement serving for the surface hysteresis loops measurements. The block schema is depicted in Fig. 5. As a source we use monochromatic red laser diode at the wavelength of 670 nm. The laser beam is linearly polarized through the polarizer P_1 and then modulated at frequency of 100 kHz using a photoelastic modulator (PEM). Final polarization before the light incidence the sample surface is given by the polarizer P_2 that is adjusted either to s or p linear polarization. The laser beam is focused almost to a point with a diameter of 0.3 mm and incidents on the sample at an angle of 45°. In this configuration, the reflected light brings information about the sample magnetization

from a depth approximately tens of nanometers. Magnetic field was generated using air coil that is situated around the sample. The magnetic field is parallel to the plane of the sample and the whole system is adjusted to measure the longitudinal magnetization component M_L. After the beam reflection the light is elliptically polarized and contains information about magnetization of the sample surface. The reflected beam passes through a Wollaston prism that splits reflected light into two orthogonal beams with different intensities. These two beams are detected by two separate PIN detectors. Their difference signal is proportional to the angle of Kerr rotation. PIN detectors are connected to Lock-in amplifier, which transmits only the signal set at 100 kHz, which is modulated by PEM.

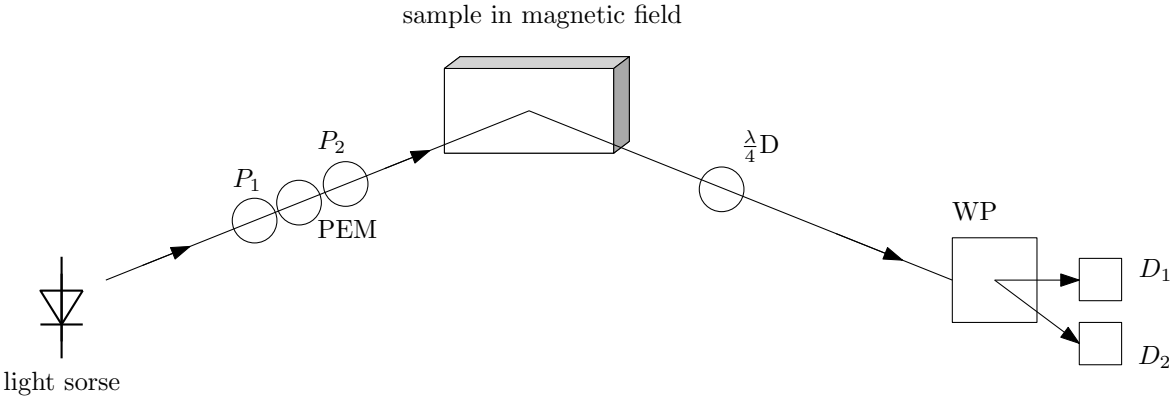

Figure 5: Block scheme of the surface magnetization measurements

The second applied method is based on the magneto-optical Kerr microscopy. This method allows to study the magnetic domain structure of the surface and uses a specially designed polarizing microscope ZEISS. As a source of light a white Xe lamp is used. Light from the lamp passes through the aperture diaphragm, a polarizer and is focused on the sample by a polarizing objective. After reflection the light goes through the analyzer, which is almost crossed with the polarizer. As the result we obtain high contrast allowing observation of magnetic domain structure. Position of the aperture diaphragm ensures sensitivity to all three components of magnetization: longitudinal, transversal and polar. For this study, the microscope is used in longitudinal sensitivity, that allows the best observation of the domain structure. An external magnetic field was

generated using magnetic coils placed around the sample holder of the microscope. Distribution of magnetic field is so that maximal intensity is on the sample and minimal intensity is close to the objective. Microscope is equipped with an ocular for visual observation of the human eyes and domain observations are performed using the CCD camera and special software. For measurements firstly we apply external magnetic field necessary to saturate the sample and the picture of the surface is stored in the PC memory. The saturated value is estimated from the hysteresis loop setup mentioned above. Then the amplitude of magnetic field is gradually decreased and we observe difference image between the saturated and actual pictures. This approach allows to visualize magnetic domains at different values of magnetic field.

It should be noted that Kerr microscopy is highly sensitive to the surface roughness of the ribbons. Domains are usually observed on the air ribbon side with lower roughness, while the air pockets and the surface of the copper wheel are responsible for higher irregularities on the wheel ribbon side that block the domain observations. We do not apply mechanical polishing of the sample surface, because this process markedly changes the surface properties.

2.6 Vibrating sample magnetometer

Vibrating sample magnetometer (VSM) manufactured by EG&G Princeton Applied Research was used for magnetic and thermomagnetic measurements. The equipment is designed for the study of the bulk magnetic properties of the materials. The VSM measures the total magnetic moment of the material and its principle is based on the Faradays law of electromagnetic induction, as seen in Fig. 6.

The sample is placed in the external magnetic field of the electromagnet and vibrates at frequency of 50 Hz. The moving sample evokes changes in magnetic flux and consequently a voltage is induced in the closely placed pick-up coils [13]. The induced voltage is proportional to

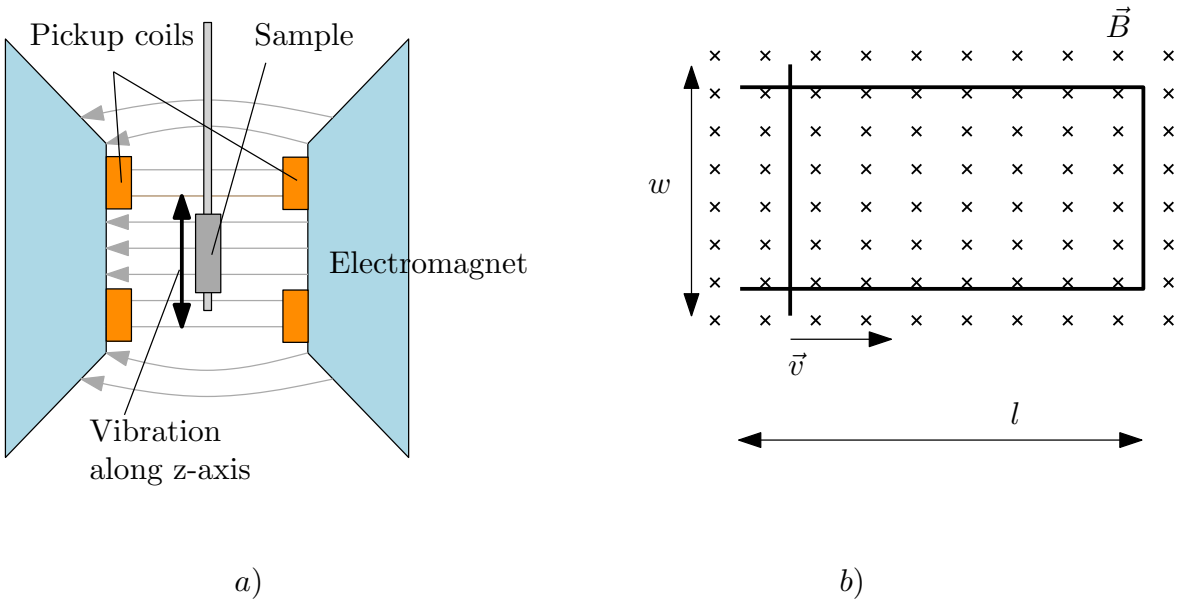

Figure 6: Schematic description of the VSM (a) and the illustration of the Faraday's law of electromagnetic induction (b)

the magnetic moment of the sample. A dependence of an induced voltage on the intensity of an external field yields in magnetization curves that are one of the most important characteristics obtained using the VSM. For VSM experiments the samples were in a form of discs with the diameter of 3 mm. The external field was changed in the interval $\pm$ 800 kA/m and the measurements were done at the room temperature.

Equipment of the VSM allows also to provide the thermomagnetic measurements, where we investigate magnetic moment of the sample as a function of the temperature. In the presented thermomagnetic curves the temperature is changed from the room temperature up to 1100 K and back during the applied constant external magnetic field of 0.005 T. The temperature increase was 4 K/min and the measurement was done under vacuum of approx. 10 mPa.

2.7 Mössbauer spectroscopy

Mössbauer spectroscopy (MS) is a non-destructive analytical method for a study of the bulk and surface hyperfine microstructure of the solid materials. This method is based on the effect of nuclear resonance fluores-

cence discovered by R. Mössbauer in 1958 [14]. It involves the resonant and recoilless emission absorption of γ–ray by atomic nuclei bound in a solid.

In general, gamma rays are produced by nuclear transitions from an unstable high–energy state, to a stable low–energy state. The energy of the emitted gamma ray corresponds to the energy of the nuclear transition (14.4 keV for ^{57}Fe used in our experiments), minus an amount of energy that is lost as recoil to the emitting atom. If the lost "recoil energy" is small compared with the energy linewidth of the nuclear transition, then the gamma ray energy still corresponds to the energy of the nuclear transition, and the gamma ray can be absorbed by a second atom (Fe) of the same type as the first. This emission and subsequent absorption is called resonance. Additional recoil energy is also lost during absorption, so in order for resonance to occur the recoil energy must actually be less than half the linewidth for the corresponding nuclear transition.

The result of Mössbauer measurement is a spectrum characterized by hyperfine parameters: intensity, I, magnetic and electrical splitting, Δ, and chemical (isomer) shift, δ. Such spectrum can consist of one up to six lines in dependence on the magnetic state of sample, its chemical composition and crystal structure.

The Mössbauer measurement can be done in transmission geometry or in backscattering geometry. If the γ–rays from the Mössbauer source come through the thin (max. 50 μm) sample and modified γ–rays are detected by detector, we speak about the transmission geometry. In such a way we obtain information from a bulk of material. But the γ-rays can strike on the surface of thick sample and the modified γ–rays are backscattered from the surface and detected by detector of a special construction, which is placed in front of a sample. Then we speak about the backscattering geometry, which allows to observe surface properties up to approximately 25 μm. Except the γ–rays the Mössbauer effect is related also to conversions electrons having the energy of 7.4 keV and

escaping from the thin surface layers of about 200 nm.

For our study the measurements were done in the transmission geometry using γ–rays (TMS), and in the backscattering geometries using γ–rays (γ–BMS), and by conversion electrons (CEMS). The measurements were done at room temperature (RT) using a ^{57}Co(Rh) source. The calibration of velocity scale was performed with α–Fe and isomer shifts are given with respect to the RT Mössbauer spectrum of α–Fe. It is therefore that hyperfine parameters of pure α–Fe are known. The α–Fe has cubic structure so the surroundings of Fe atoms are symmetric and no quadrupole (electrical) splitting exists. Moreover, the crystal structure is formed only by Fe atoms and the measurements are done by ^{57}Fe the chemical (isomer) shift is also zero. All spectra were evaluated within the transmission integral approach using the program CONFIT used in Mössbauer laboratory at the Institute of Physics of Materials in Brno. The amorphous structure is represented by Gaussian distributions of hyperfine induction reflecting various chemically and topologically disordered surroundings of resonating iron atoms. A usage of Mössbauer spectrometry using iron isotope is conditioned by a presence of iron atoms in a sample. TMS could be done on both SLF and BL samples, but the results of transmission measurement of BL sample yield information only from the interlayer and the FeSiB side. Similarly, the backscattering geometry using conversion electrons (CEMS) could be used for surface observations of the SLF sample and of the BL sample from the Fe–side. The backscattering geometry using γ–rays was used for the air side of the SLF sample and for both sides of the BL sample. The reason for the measurement of BL sample from the Co-side was that the penetration depth of the γ–rays is approximately 25 μm. Therefore on condition that an approximate thickness of Co–based layer is 15 μm and the thickness of interlayer 6 μm it could be awaited that measured spectrum will reflect the microstructure of interlayer partly influenced by a small portion of FeSiB layer from the opposite side of BL sample.

3 Results and discussion

3.1 Structure

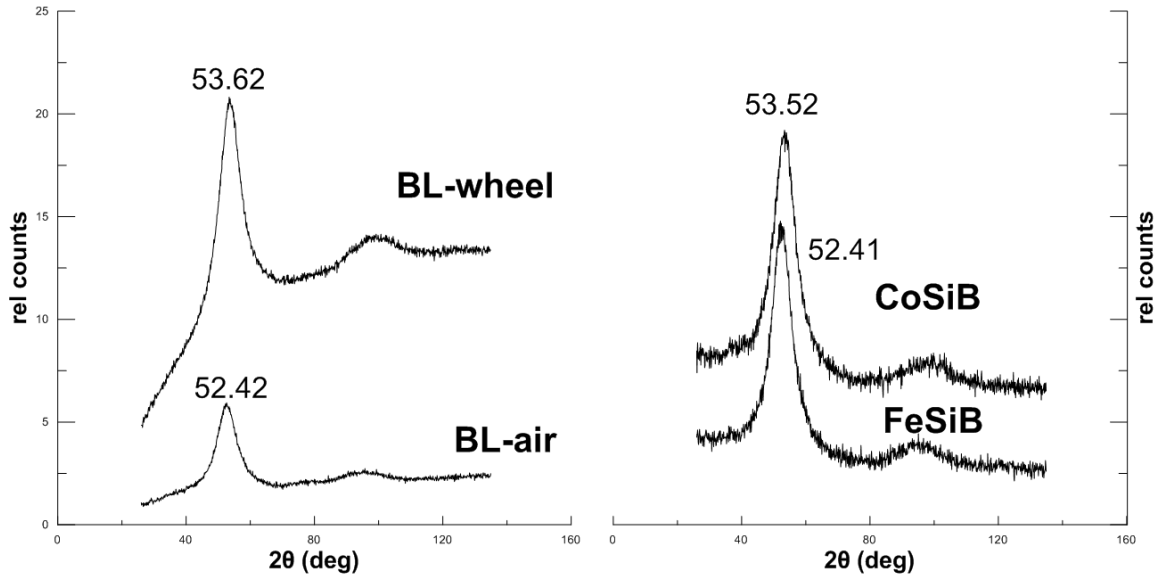

Figure 7: X–ray diffraction patterns

The Fig. 7 shows the results of X–ray diffraction measurements from both sides of BL sample and from the corresponding sides of SL samples. An absence of sharp peaks at diffractograms confirms that the ribbons have amorphous structure. The peaks of the curves representing the Co-side of the BL sample and the SLC sample, 53.62 deg and 53.52 deg, respectively, agree well each other similarly as the peaks for opposite Fe-side (BL) and FeSiB sample. They are only shifted slightly to higher 2θ.

3.2 Scanning electron microscopy and concentration profiles

High resolution scanning electron microscopy (HRSEM) was applied for structural observations of the cross-section of the the BL sample only. The result is shown in Fig. 8 and in more detail in Fig. 9.

The upper part corresponds to CoSiB layer, and the bottom layer is FeSiB. It is clearly seen that the surface at the Co-rich side of the BL

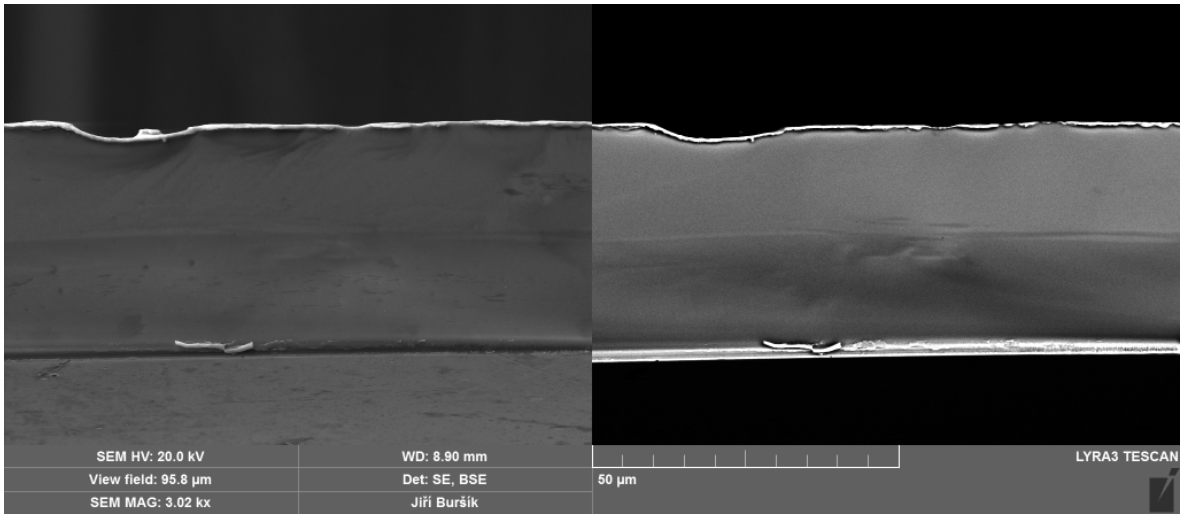

Figure 8: Results from scanning electron microscopy

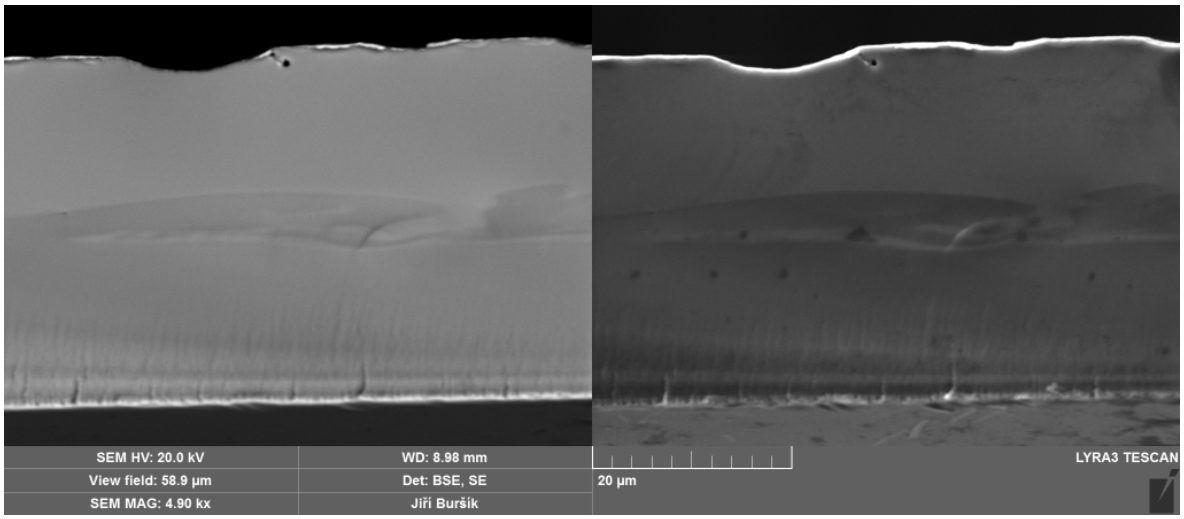

Figure 9: Detail picture of bilayered ribbon obtained using scanning electron microscopy

sample being in contact with wheel is rough. The image was done using Back Scattering Electron (BSE) detector and Secondary Electron (SE) detector. From the figures the interlayer is well seen but its thickness is not homogeneous. It was between 2 μm up to 6 μm. Moreover, this investigation has confirmed the amorphous structure of both layers because no nanocrystals are seen. This was also confirmed by XRD measurements.

The chemical analysis across the ribbon sample, done in direction from the Co-side to Fe-side, is displayed in Fig. 10. The analysis was done with 2 μm steps. Using SEM it was not possible to detect the

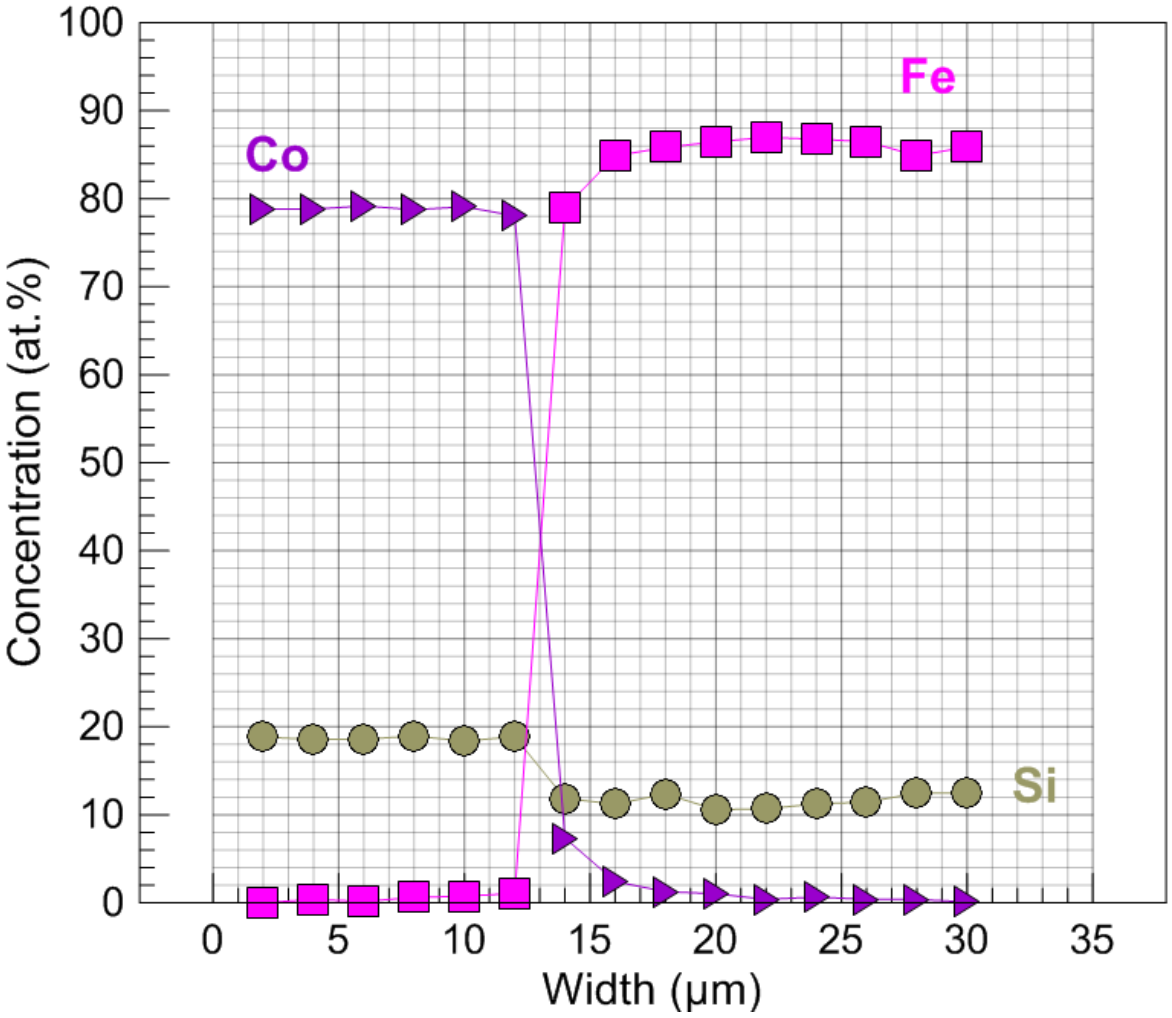

Figure 10: Element distribution in the bilayered ribbon

boron content in the material. Therefore the Fig. 10 shows only the relative changes of Co, Fe, and Si elements. Nevertheless the obtained distribution of detected elements is in good agreement with nominal concentration on [4].

3.3 Bulk magnetic properties

The next results were obtained using VSM described in section 2.6. The Fig. 11 shows the hysteresis loops of the BL and both SL samples.

The hysteresis loops depicted in Fig. 11a show the changes in magnetization with an applied magnetic field ± 800 kA/m that is sufficient to saturate all samples. To see the hysteresis curves close to zero field they were depicted also in the smaller range of external field in Fig. 11b.

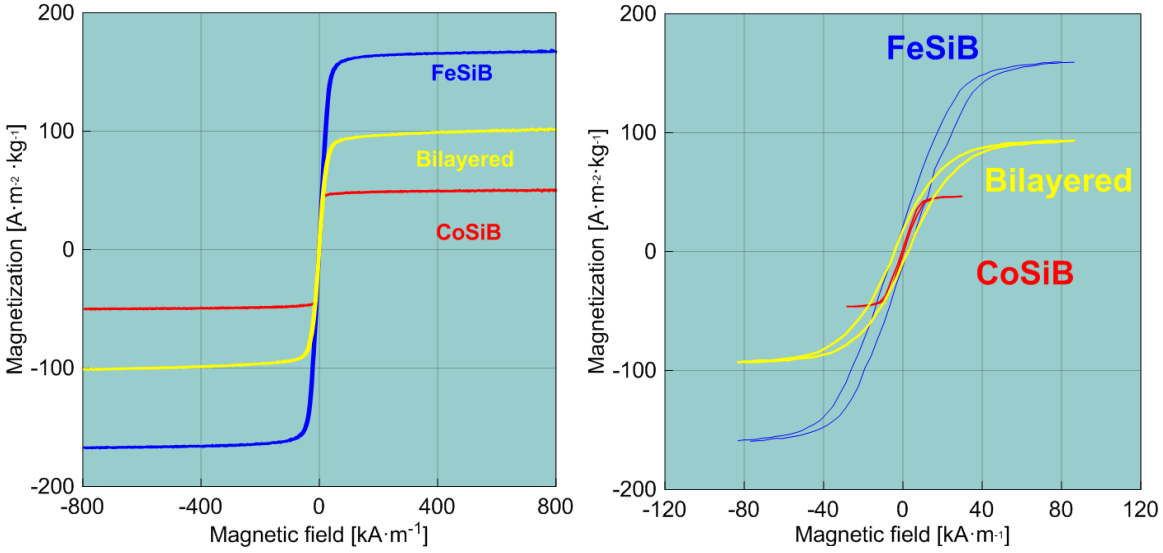

Figure 11: VSM hysteresis loops

The magnetic characteristics obtained from the VSM measurements are then summarized in Table 1.

Table 1: The values of coercivity H_c and remanent magnetization M_r

	Coercitive field H_c (kA/m)	Remanent magnetization M_r ($\mathrm{A \cdot m^2/kg}$)
CoSiB	0.9	3.08
FeSiB	3.6	16.85
Bilayered	3.2	13.58

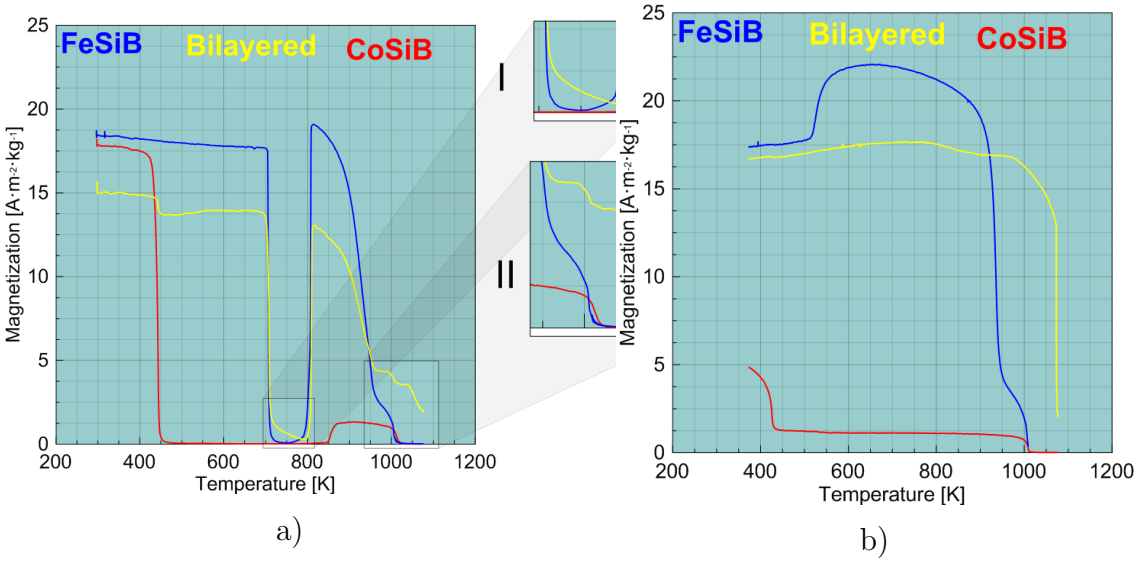

Figure 12: Thermomagnetic VSM curves

The changes of magnetization in dependence on the increasing (left side - a) and decreasing (right side - b) temperatures are depicted in Fig. 12. The first decrease in the BL samples corresponds well with a decrease in magnetic moment the SLC sample. The decreasing of magnetization of SLC sample means that SLC and BLC transform from a ferromagnetic state to a paramagnetic state. The Curie temperature of 443 K is substantially lower as presented for as-quenched CoSiB wires of the same composition in Ref. [15] but in good agreement with those obtained in Ref. [5]. Above approximately 450 K the BL sample follows the magnetic behavior of SLF sample what is due to a presence of the active FeSiB layer on the air side. When the temperature achieves the value of approximately 706 K the magnetization of BL ribbon decreases like the magnetic moment of the SLF sample. This is the temperature of the ferromagnetic-paramagnetic transition of the FeSiB corresponding to Curie temperature in Refs. [16, 17]. Above the temperature of 706 K the difference in thermomagnetic curves of BL and SL samples can be observed. This difference is shown in detail in Fig. 12 (part I). At the temperature of 763 K the SLF sample begins to crystallize and its magnetization increases due to formation of the magnetic Fe(Si) phase. The situation in the BL sample is more complicated because its magnetic state is influenced also by magnetic properties of the FeCoSiB interlayer. Nevertheless the FeSiB layer begins to crystallize as well and the magnetization of BL sample begins to rise at 800 K. The crystallization temperature of SLC sample is approximately 847 K. This behavior is in good agreement with studies of the amorphous $(Fe_{1-x}Co_x)SiB$ alloys yielding an increase of crystallization temperature with increasing Co content [18]. In the temperature range between 900 K and 1100 K the transitions of the crystalline phases on the wheel side (Co(Si), Co-B) as well as on the air side (FeSi, Fe-B) into paramagnetic states follow the corresponding transitions detected in pure SLC and SLF crystallized samples (part II). Moreover, additional Curie temperature at approx. 1057 K corresponds to transition of crystallized interlayer into paramagnetic state. It is supported by the first-principles predictions of the Curie

temperatures yielding visibly higher value for the bcc-FeCo in comparison to pure bcc-Co and bcc-Fe [19]. The changes of magnetization of the crystallized BL sample at decreasing temperature do not follow the thermomagnetic curves of crystalline FeSiB and CoSiB samples [10]. It is caused by a complicated phase composition of BL sample after crystallization that should be clarified in the next studies concerning this BL ribbon.

Fig. 13 and Table 2 show the magnetic properties of the samples after thermomagnetic measurements.

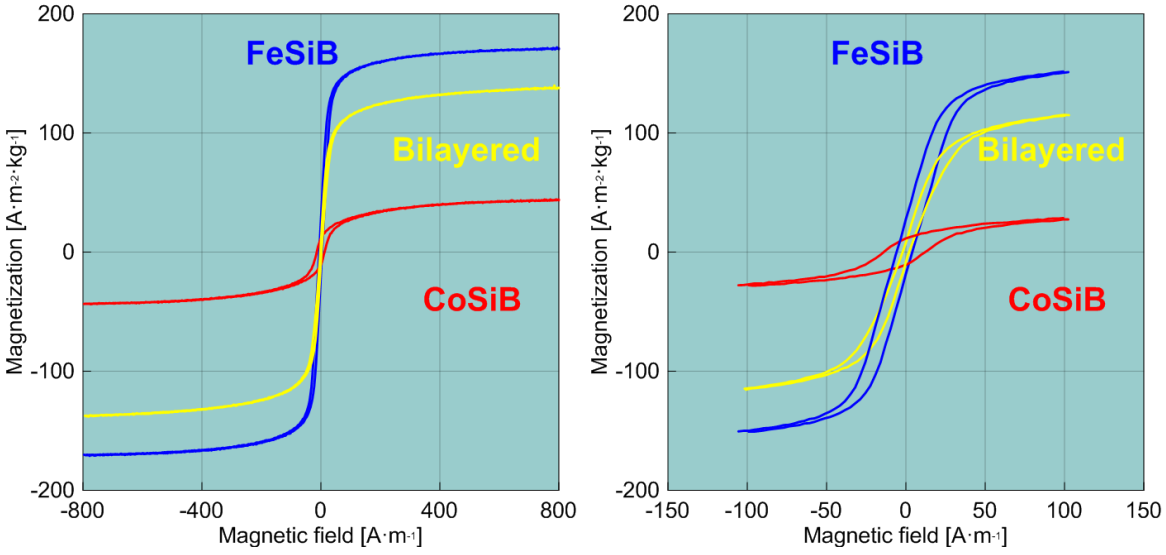

a) b)

Figure 13: Magnetic hysteresis loops of samples after thermomagnetic measurements

Similarly as in case of the BL and SL samples in the initial states, the Fig. 13a shows the saturated hysteresis loops while Fig. 13b shows the curves close to the zero field. Nevertheless both parts of the Fig. 13 as well as obtained magnetic parameters in Table 2 yield magnetic hardening of all samples caused by crystalline phase.

A comparison of the results shown in Fig. 11, 12, 13 and Tables 1 and 2 documents that the magnetic behavior of BL sample is more influenced by magnetic properties of the BLF side.

Table 2: Magnetic parameters of ribbons after thermomagnetic measurements

	Coercitive field H_c (kA/m)	Remanent magnetization M_r ($\mathrm{A \cdot m^2/kg}$)
CoSiB	13.1	11.14
FeSiB	4.1	22.99
Bilayered	2.1	8.98

3.4 Surface magnetic properties

The Fig. 14 shows the hysteresis curves measured by MOKE apparatus at SL and BL samples. The key parameter is in this case the surface magnetic anisotropy that reflects shapes and inclinations of measured hysteresis loops. It is evident that their magnetic behavior strongly depends on the type (SL, BL) and side (air, wheel) of the ribbon. Fig. 14a shows the curves of SLF sample that were obtained by focusing laser spot in two different places on the ribbon surface. The different shape of loops documents the presence of two magnetic phases that can correspond either to the amorphous FeSi and FeB clusters coming from different sample depths [20] or they could originate also from the amorphous sample and thin ferromagnetic oxide on its surface. The separated oxide islands were detected by Raman microspectroscopy and are shown in Fig. 15 on the right panel. The left panel shows the spectrum with the peaks at 214.6, 273, and 385.2 $\mathrm{cm^{-1}}$ of the Raman shifts corresponding well with those obtained for the reference spectrum of Fe_2O_3 [10].

As concerns a shape of the surface hysteresis curves and the bulk hysteresis curves (VSM), it's necessary to note that both are influenced by different conditions of experiments. MOKE method is very sensitive to small and thin regions. It can detect different clusters in the surface of the material, which are then shown on hysteresis curve. VSM reflects integrated magnetic properties of the whole material and it is not able to distinguish magnetically different surface phases in the SLF sample. Therefore the shapes of the surface and bulk hysteresis curves are different [21].

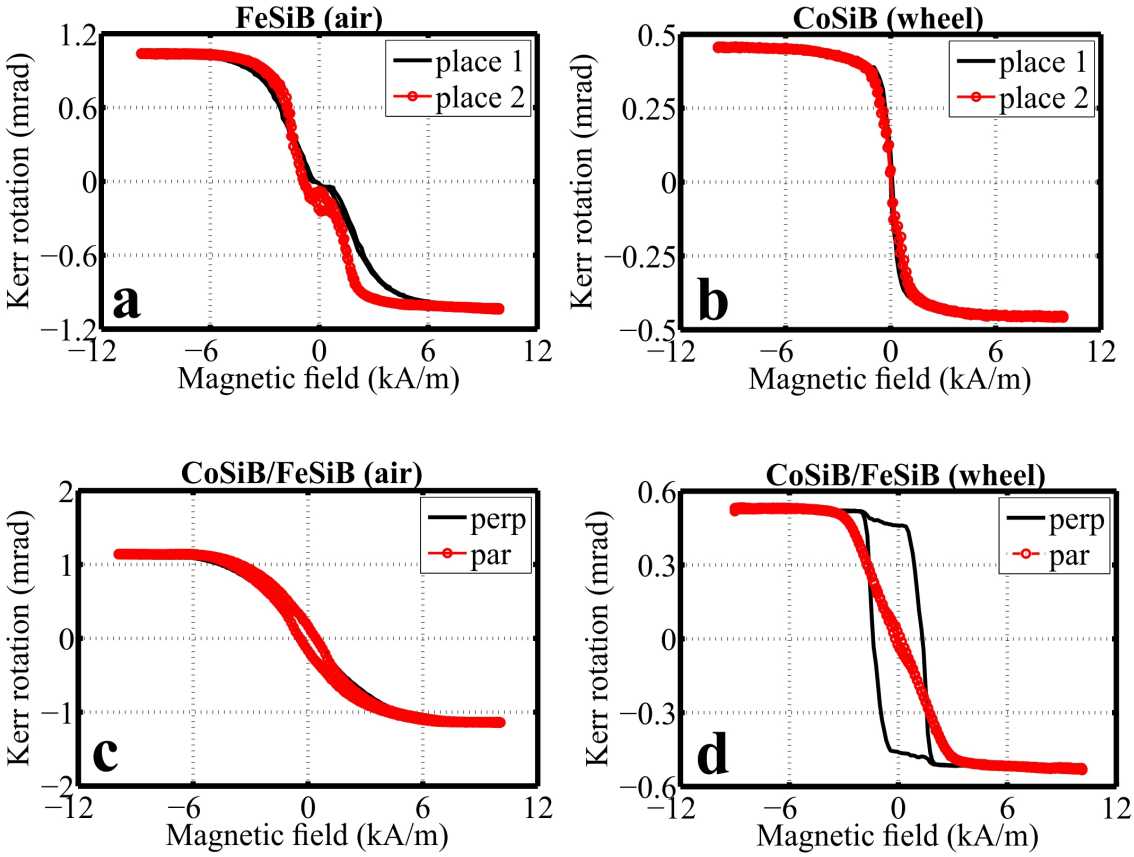

Figure 14: MOKE surface hysteresis loops

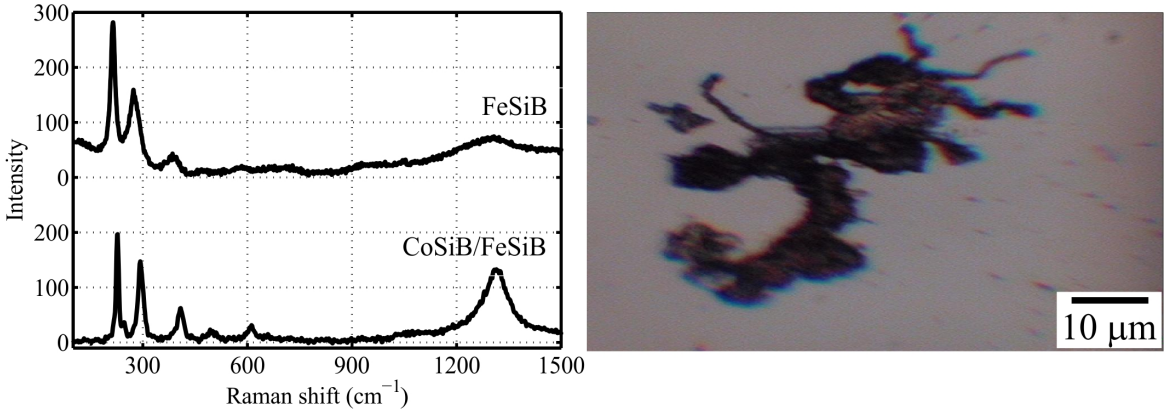

Figure 15: Iron oxide spectra obtained from the air side of FeSiB and CoSiB/FeSiB ribbons (left) together with the microscopic image of detected Fe_2O_3 area (right)

The second method based on Kerr effect was magneto-optical Kerr microscopy allowing domain structure observations. Fig. 16a shows the domain pattern taken from the air side of the SLF sample. Two types of domains are present. The wide curve domains, having origin in the local tensile stresses as a consequence of sample preparation. They follow the in-plane easy magnetization axis, while the fine fingerprint domains

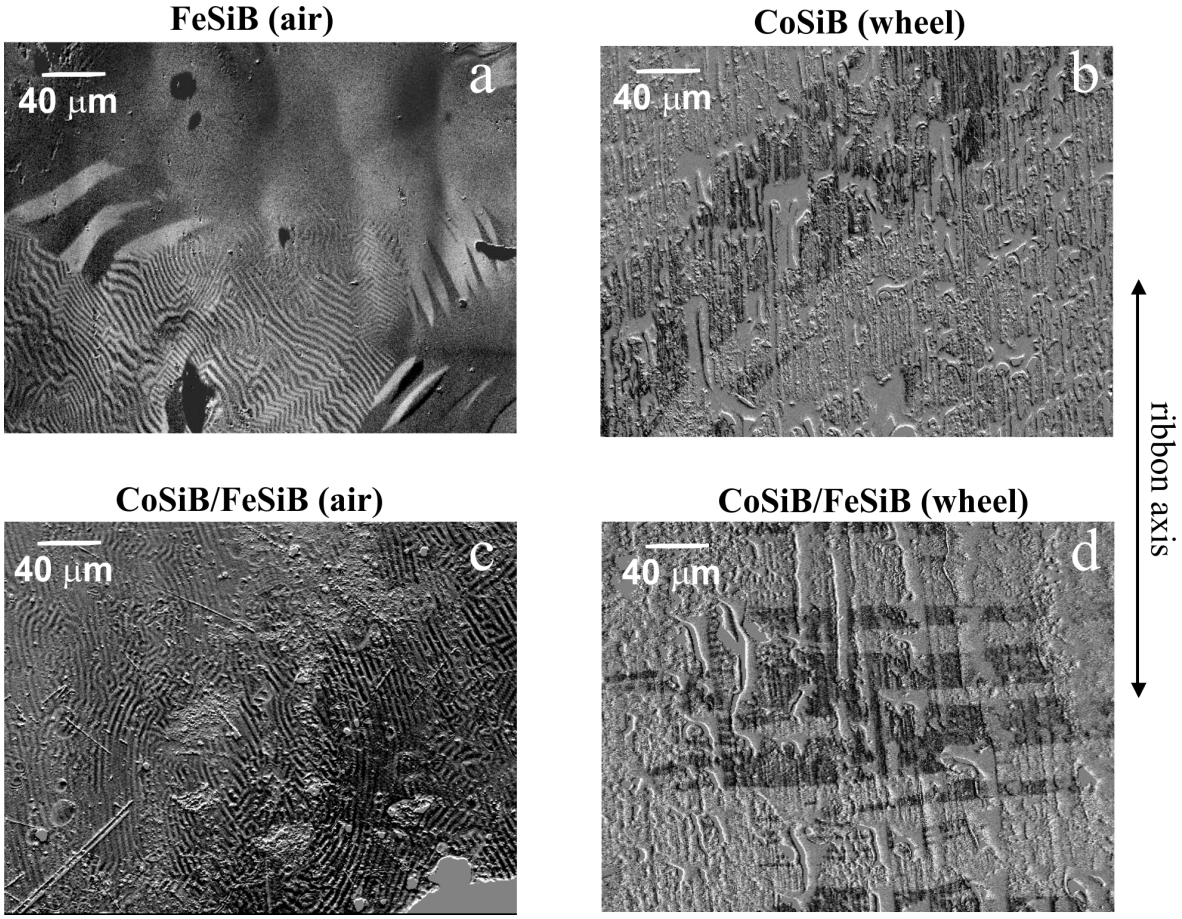

Figure 16: Observed domain patterns

are the surface closure domains indicating a presence of perpendicular anisotropy due to a compressive stress. Observed differences in local magnetic properties are supported by the surface hysteresis loops in Fig. 14a [10].

To compare the magneto-optical observations of both surfaces of BL sample with the corresponding surfaces of SL samples, the CoSiB sample was studied from the wheel side. The surface roughness is much higher according to the observed air surface of FeSiB sample and therefore obtaining domain patterns was more complicated. The air pockets and other jogs on the surface overlap observed magnetic domains and cause their fuzziness. No fingerprint domains are visible (Fig. 16b) and magnetization lies in the ribbon plane. The hysteresis loops (Fig. 14b) taken from different sample places yield the same shape and they mutually overlap. In general we can say that gradient of tensile stresses is much lower than in FeSiB alloys. As a result the easy magnetization

axis slowly fluctuates along the ribbon surface and changes in its inclination are not detected. The Raman spectroscopy did not evidence any oxidation [10].

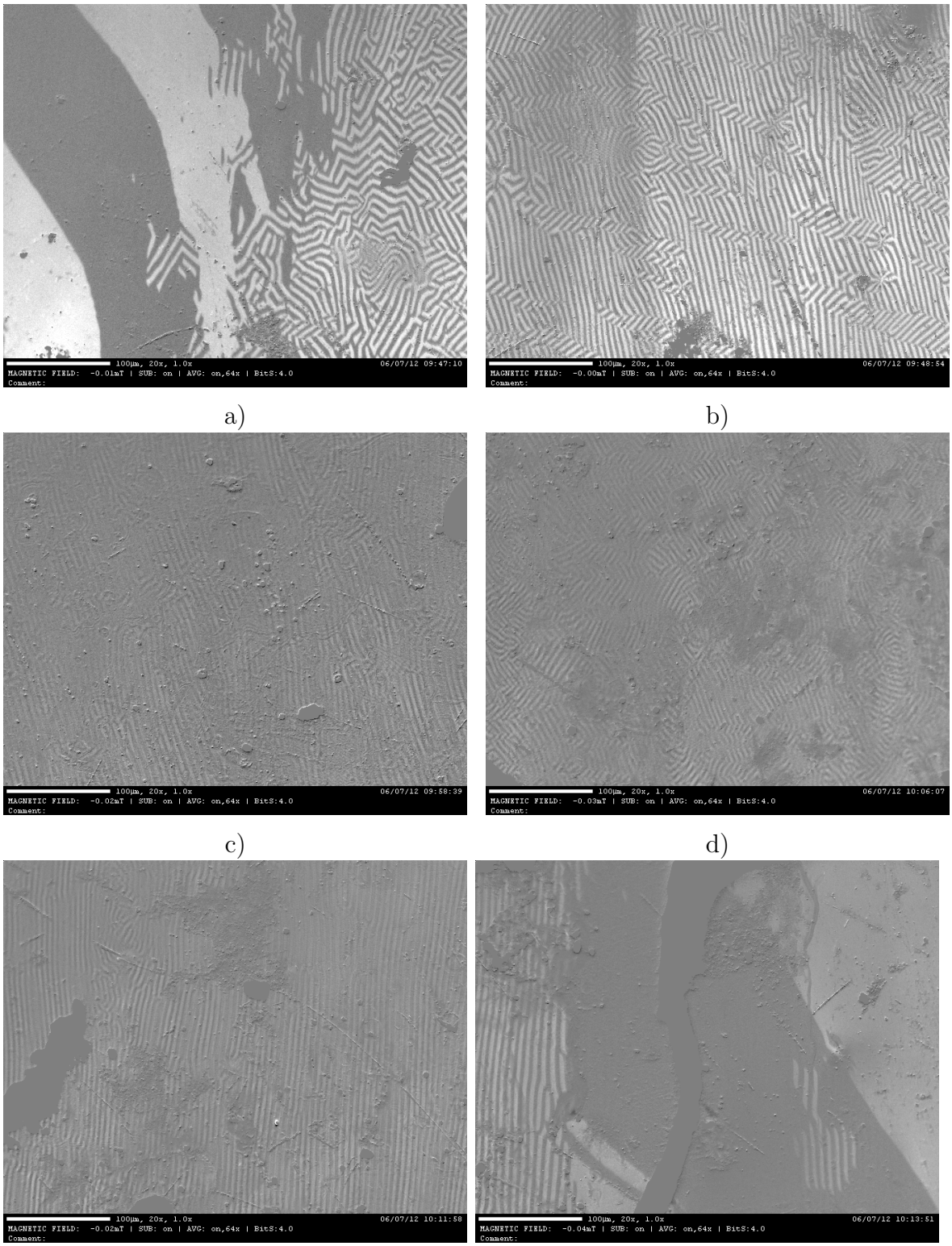

Figure 17: Surface magnetic domains measured across the width (from left (a) to right (f) edge) of BLF ribbon

Quite different surface magnetic properties are observed for BL sample. The coiled sample with high level of internal stress was fixed on the planar sample holder. This has induced the additional inhomogeneous anisotropy reflecting the compressive stress on the air side and tensile stress on the wheel side. This is the reason of detecting the strong perpendicular anisotropy on the air surface documented by a presence of only fingerprint domains (Fig. 16c) and by hysteresis loops (Fig. 14c) with very slow magnetization reversal (anisotropy field H_a is about 6 kA/m) if the magnetic field is applied along the ribbon axis in the sample plane. Moreover, a rotation of the square sample within 90° does not cause any change of the shape of the loop and the value of H_a remained practically identical. This is a clear indication of the perpendicular direction of the easy magnetization axis with respect to sample surface. The surface oxidation (Fig. 15) was detected only on the Fe-rich surface. All the peaks correspond again to Fe_2O_3 [10].

Investigation of anisotropy behavior across the air side of BLF sample is shown in Fig. 17. It is seen that the strength of compressive stress is different in various sample places. In the middle of the ribbon we observe small fingerprint domains indicating strong perpendicular anisotropy. By gradual moving toward the sample edges the fingerprint domains become larger and close to the edge are replaced by the wide in-plane domains indicating presence of tensile stress. Therefore, ribbon unbending on the planar sample holder is responsible for inducing of inhomogeneous anisotropy not only in the ribbon depth, but also across the surface of BLF ribbon.

In-plane uniaxial anisotropy with a certain position of the easy axis of magnetization can be detected on the wheel side of the BL sample. Easy axis orientation with regard to the applied magnetic field can be estimated either from the directions of measured strip domains or from the measured hysteresis loops using the relation $\alpha = \arccos(M_r/M_S)$, where M_r and M_S are remnant and saturated magnetizations, respectively. Therefore, it is evident (Figs. 16d and 14d) that it lies in the sample

plane perpendicular to the ribbon axis. Our explanation is based on the fact that measured piece of ribbon is predominantly coiled along the ribbon axis. After ribbon unbending the tensile stress is induced in the ribbon axis which, together with negative magnetostriction coefficient, is responsible for inducing the hard magnetization axis in this direction. On the other hand, if the coiling of the sample in lateral and transverse direction produces stresses of a comparable intensity, the resulting tensile stress induces very probably the in-plane easy magnetization axis more or less inclined from the ribbon axis [10].

In conclusion of this section we can state that behavior of perpendicular anisotropy on the surface of BLF sample and in the whole ribbon volume (VSM) is not identical. Bulk hysteresis loop of BL ribbon shows that the sample cannot be saturated in the external field of 8 kA/m, contrary to the MOKE results. It means that perpendicular anisotropy observed on the air side becomes stronger as getting deeper under the surface and it overlaps a response from the in-plane anisotropy on the wheel side. This conclusion is in good agreement with Mössbauer measurements of BL samples (see next section) yielded the difference in magnetic moments orientation due to connection of two materials with different magnetostriction coefficients [10].

3.5 Mössbauer spectroscopy

Fig. 18 shows the spectra obtained by Mössbauer measurements. The left panel in Fig. 18 shows FeSiB sample and the middle panel shows BL sample. In both cases the upper parts (a) correspond to surface CEMS measurements: for BL sample it was from the Fe-side and for the SLF sample from the air (shiny) side. The lower parts (b) correspond to TMS measurements (bulk properties). The right panel shows the γ–BMS results obtained for the BL sample from the air Fe-(a) and the wheel Co-side (b), respectively. As seen from the Fig. 18 (left panel) the shapes of both CEMS and TMS spectra of the SLF sample are very similar. This reflects that there is no visible difference between the bulk and the

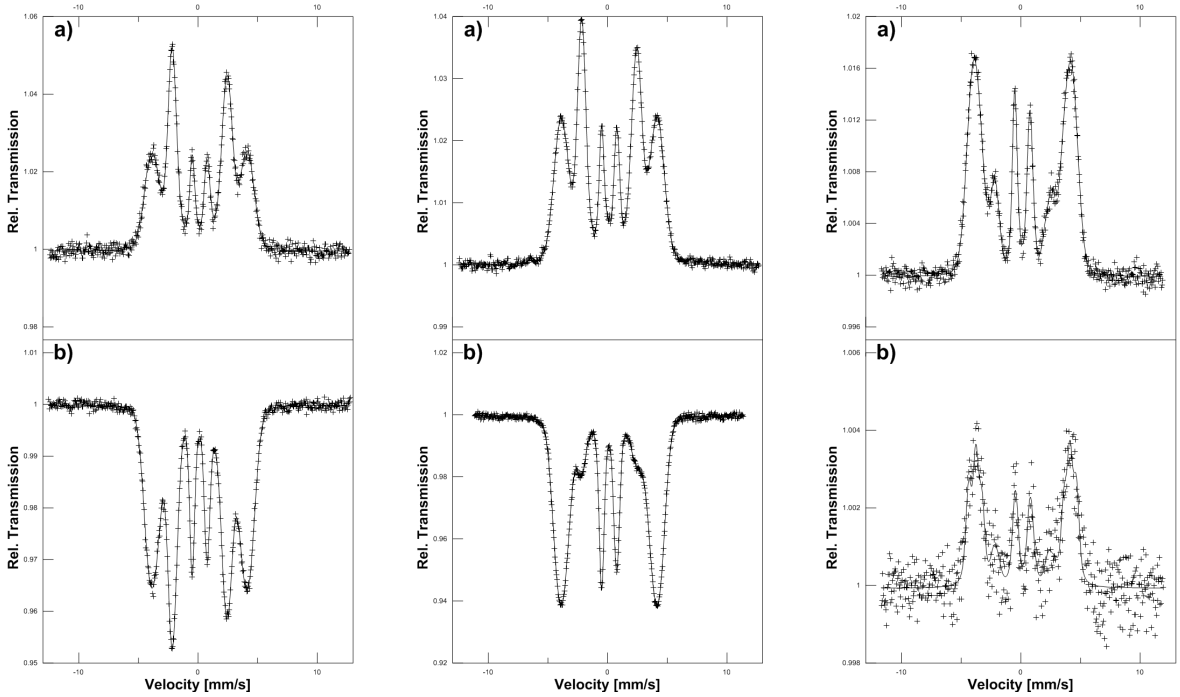

Figure 18: Mössbauer spectra of the SLF sample (left panel) and the BL sample (middle and right panel)

surface of the SLF. Because we have used ^{57}Fe Mössbauer spectrometry and the SLC sample does not contain any Fe atom in its structure, the measurements of this sample and similarly the Co-side of the BL sample by CEMS are impossible.

The measurements of BL sample were made from the both sides using γ–BMS. The reason for measurement also from the Co-side was, that the modified backscattered γ–rays comes from a depth of approximately 25 μm which means that approximately 15 μm of the CoSiB layer is for Mössbauer effect invisible but the backscattered γ–rays from the Fe-CoSiB interlayer (6 μm) and partly from the opposite Fe-side can be detected. Therefore the upper spectrum (a – right panel) reflects the Fe-side of BL sample and the spectrum bottom (b) represents predominantly the interlayer slightly influenced by FeSiB layer.

The spectra were fitted by distributions of hyperfine inductions and the selected parameters are summarized in Table 3. The individual distributions reflect chemical and topological disorder of an amorphous structure. The relative intensities of lines in the sextuplet depend on

an angle θ between the incident γ–ray beam and magnetic moments according to well known relation:

$$I_{1,6} : I_{2,5} : I_{3,4} = \frac{3}{4}(1 + \cos 2\theta) : \sin 2\theta : \frac{1}{4}(1 + \cos 2\theta)$$

In a case of fully random ordered magnetic moments we obtain:

$$I_{1,6} : I_{2,5} : I_{3,4} = 3 : 2 : 1$$

which means that the ratio of the second(fifth) to first(sixth) (D_{21}) is 0.66. A decrease of (D_{21}) to zero reflects an ordering of magnetic moments parallel to the γ–ray beam. In present case the magnetic moments in the FeSiB sample and at the Fe-side surface of BL sample are oriented nearly randomly ((D_{21}) ranges between 0.8 and 1.05) while in the bulk of BL sample the (D_{21}) reaches the value of 0.14 (TMS). The values of 0.25 in the γ–BMS spectrum obtained from the Fe-side, and again 0.12 in the γ–BMS obtained from the Co-based side document a change of magnetic moment orientation nearly parallel with direction of the γ–rays. This can be ascribed to creation of stresses due to connection of two materials differing in magnetostriction coefficients.

Table 3: The mean values of hyperfine parameters corresponding to analysis of the Mössbauer spectra shown in Fig. 18; hyperfine induction B, width of distribution ΔB, isomer shift δ, quadrupole splitting Δ, and ratio of the second and first line of sextuplet D_{21}.

Sample (geometry of meas.)	B (T)	ΔB (T)	δ (mm/s)	Δ (mm/s)	D_{21} -
FeSiB (TMS)	24.13(40)	6.61(69)	0.135(16)	-0.024(12)	0.081
(CEMS, air side)	24.55(4)	7.90(6)	0.107(19)	-0.024(6)	1.247
CoSiB/FeSiB (TMS)	24.30(23)	6.95(36)	0.112(36)	-0.027(19)	0.138
(CEMS Fe-side)	24.29(9)	10.83(16)	0.112(25)	0.029(11)	1.052
(γ-BMS Fe-side)	24.81(59)	5.88(91)	0.134(126)	-0.027(78)	0.251
(γ-BMS Co-side)	24.85(13)	7.33(38)	0.141(14)	-0.015(26)	0.115

4 Conclusions

The combination of different methods with different sensitivity to the surface and the bulk offers a possibility for the detail and comprehensive study of the structure and magnetic properties of the relatively new bilayered soft magnetic material prepared by planar flow casting in the ribbon form. The additional investigations of the single-layered ribbons of the corresponding compositions allow comparing their properties with properties of the BL ribbon. This could be useful for reversal verification of the production process with respect to obtain desirable properties of bilayered ribbon type materials.

Comparison the obtained results for the CoSiB/FeSiB BL ribbon with results for the CoSiB and FeSiB SL ribbons has shown that the BL ribbons are predominantly influenced by the properties of the more magnetostrictive FeSiB alloy. The magnetic and Mössbauer measurements of the bilayered sample yielded that the perpendicular anisotropy observed on the air side becomes stronger as getting deeper under the surface and overlaps in-plane anisotropy from the wheel side. Moreover it was found that the interconnection of two materials of different magnetostriction behavior and formation of diffuse interlayer bring new features potentially available for sensing elements. Magnetic sensors using the low-frequency driving current will reflect mainly the bulk magnetic properties, while the response on the currents with higher frequencies will correspond to the presented surface magnetic properties.

In future we plan to continue in the research of bilayered CoSiB/FeSiB ribbons and to improve their soft magnetic properties by additional annealing at different times and temperatures. Our aim is to find the optimized bilayered alloy with the lower coercivity, higher magnetization effect from the viewpoint of the surface and bulk, and suitable magnetic anisotropy.

References

[1] P. Duwez, R. H. Willens, W. Klement. Continuous series of metastable solid solutions in silver-copper alloys. *Journal of Applied Physics*. 1960, vol. 31, pp. 1136-1137.

[2] W. Klement, R. H. Willens, P. Duwez. Non-crystalline structure in solidified gold-silicon alloys. *Nature*. 1960, vol. 187, pp. 869-870.

[3] K. Suzuki, H. Fujimori, K. Hashimoto. *Amorphous metals*. Moscow, Metalurgija, 1987. 328 p.

[4] A. Mitra, R.K. Roy, B. Mahato, A.K. Panda, G. Vlasák, D. Janičkovič, P. Švec Sr. Development of FeSiB/CoSiB bilayered melt-spun ribbon by melt-spinning technique. *Journal of Superconductivity Novel Magnetism*. 2011, vol. 24, pp. 611-615.

[5] I. Maťko, P. Švec, P. Švec Sr., D. Janičkovič, M. Stoica, T. Gemming. Preparation of rapidly quenched bilayered ribbons, their properties and interface structure. *Proc. 17th Int. Conference on Applied Physics of Condensed Matter., J. Vajda, I. Jamnický (eds.)*. 2012, pp. 145-148.

[6] M. Konč, T. Švec, A. Zeleňáková, P. Sovák, P. Kollár. The structure and magnetic properties of Fe–Cu–Nb–Si–B/Fe–Nb–Si–B bilayer. *Czechoslovak Journal of Physics*. 2002, vol. 52, pp. 195-198.

[7] K. Mohri, T. Uchiyama, L. P. Shen, C M. Cai, L. V. Panina, Sensitive micro magnetic sensor family utilizing magneto-impedance (MI) and stress-impedance (SI) effects for intelligent measurements and controls. *Sensors and Actuators A*. 2001, vol. 91, pp. 85-90.

[8] L. Mehnen, H. Pfutzner, E. Kaniusas. Magnetostrictive amorphous bimetal sensors. *Journal of Magnetism Magnetic Materials*. 2000, vol. 215-216, pp. 779-781.

[9] T. Klinger, H. Pfutzner, P. Schonhuber, K. Hoffmann, N. Bachl. Magnetostrictive amorphous sensor for biomedical monitoring. *IEEE Transactions on Magnetics*. 1992, vol. 28, pp. 2400-2402.

[10] O. Životský, A. Titov, Y. Jirásková, J. Buršík, J. Kalbáčová, D. Janičkovič, P. Švec. Full-scale magnetic, microstructural, and physical properties of bilayered CoSiB/FeSiB ribbons. *Journal of Alloys and Compounds*. 2013, in review process.

[11] R. J. Thibeau, C. W. Brown, R. H. Heidersbach. Raman spectra of possible corrosion products of iron. *Applied Spectroscopy*. 1978, vol. 32, pp. 532-535.

[12] *Great Soviet Encyclopedia*. 3.ed, Moscow, Soviet Encyklopedia, 1969. 633 p.

[13] R.Feynman. *The Feynman Lectures on Physics*. Vol 2., California, 1964.

[14] R. L. Mössbauer. Kernresonanzfluoreszenz von Gammastrahlung in ^{191}Ir. *Zeitschrift für Physik A (in German)*. 1958, vol. 151, pp. 124–143.

[15] T. Sanchez, P. Alvarez, J. Olivera, M.J. Perez, F.J. Belzunce, J.D. Santos, J.L. Sanchez, M.L. Sanchez, P. Gorria, B. Hernando. Torsion annealing influence on the impedance behavior in amorphous FeSiB and CoSiB wires. *Journal of Non–Crystalline Solids*. 2007, vol. 353, pp. 914-918.

[16] M. Fähnle. On the temperature dependence of the spontaneous magnetization in amorphous ferromagnets. *Solid State Communications*. 1984, vol. 49, pp. 391-394.

[17] T. Nagarajan, U. Chidambaram Asari, S. Srinivasan, V. Sridharan, A. Narayanasamy. Crystallization of some iron–based metallic glasses. *Materials Science and Engineering*. 1988, vol. 97,pp. 355-359.

[18] J. Filipecki, Z. Mandecki, C.F. Conde, A. Conde. Crystallization of (Fe,Co)SiB alloys: influence of relaxation processes. *Journal of Materials Science*. 1988, vol. 33 pp. 2171-2177.

[19] M. Lezaic, Ph. Mavropoulos, S. Blugel. First-principles prediction of high Curie temperature for ferromagnetic bcc-Co and bcc-FeCo alloys and its relevance to tunneling magnetoresistence. *Applied Physics Letters*. 2007, vol. 90, pp. 082504.

[20] O. Zivotsky, A. Hendrych, L. Klimsa, Y. Jiraskova, J. Bursik, J. A. M. Gomez, D. Janickovic. Surface microstructure and magnetic behavior in FeSiB amorphous ribbons from magneto-optical Kerr effect. *Journal of Magnetism and Magnetic Materials*. 2012, vol. 324, pp. 569-577.

[21] O. Životský, K. Postava, L. Kraus, Y. Jirásková c, J. Juraszek, J. Teillet, K. Barčovaá, P. Švec, D. Janičkovič, J. Pištora. Surface and bulk magnetic properties of as-quenched FeNbB ribbons. *Journal of Magnetism and Magnetic Materials*. 2008, vol. 320, pp. 1535–1540.